To be published in Applied Optics:

Title: Construction and validation of UV-C decontamination cabinets for filtering facepiece respirators

Authors: Martin Purschke,Mazzin Elsamaloty,Jeff Wilde,Nichole Starr,R. Rox Anderson,William Farinelli,Fernanda Sakamoto,Maryann Tung,Joshua Tam,Lambertus Hesselink,Thomas Baer

Accepted: 12 July 20

Posted 17 July 20

DOI: https://doi.org/10.1364/AO.401602

Construction and validation of UV-C decontamination cabinets for filtering facepiece respirators

Martin Purschke[1,2], Mazzin Elsamaloty[3], Jeffrey P. Wilde[4], Nichole Starr[5], R. Rox Anderson[1,2], William A Farinelli[1,2], Fernanda H. Sakamoto[1,2], , Maryann Tung[4], Joshua Tam[1,2,] Lambertus Hesselink[4], and Thomas M. Baer[4,*]

[1] *Harvard Medical School, 25 Shattuck Street, Boston, MA 02115, USA*
[2] *Wellman Center for Photomedicine, Massachusetts General Hospital, 50 Blossom Street, Boston, MA 02114, USA*
[3] *University of Toledo, College of Medicine and Life Sciences, 3000 Arlington Avenue, Toledo, OH 43614, USA*
[4] *Stanford University, Stanford University Photonics Research Center, 348 Via Pueblo Mall, Stanford, CA 94305, USA*
[5] *University of California San Francisco, School of Medicine, 513 Parnassus Ave, MSB, San Francisco, CA 94117, USA*
[*] *Corresponding Author: tmbaer@stanford.edu*

Abstract: We present evidence-based design principles for three different UV-C based decontamination systems for N95 filtering facepiece respirators (FFRs) within the context of the SARS-CoV-2 outbreak of 2019-2020. The approaches used here were created with consideration for the needs of low- and middle-income countries (LMICs) and other under-resourced facilities. As such, a particular emphasis is placed on providing cost effective solutions that can be implemented in short order using generally available components and subsystems. We discuss three optical designs for decontamination chambers, describe experiments verifying design parameters, validate the efficacy of the decontamination for a commonly used N95 FFR (3M, #1860), and run mechanical and filtration tests that support FFR reuse for at least 5 decontamination cycles.

1. Introduction

1.1 Statement of need

As the numbers of Coronavirus Disease 2019 (COVID-19) cases globally continue to grow at alarming rates, demand for personal protective equipment (PPE) continues to outstrip production, resulting in PPE shortages worldwide. Among the shortages of various types of PPE, the shortage of disposable N95 filtering facepiece respirators (FFRs), commonly known as N95 masks, is especially severe [1,2]. The tight seal to the face, when properly fitted, and the high filtration efficiency of the filter material make N95 FFRs a suitable choice for use in healthcare settings to protect workers from airborne transmission of infectious agents [3]. Due to recent supply chain limitations, many medical facilities are faced with difficult decisions around how to best ration their supply of N95 FFRs. For some, their strategy has included the decontamination and reuse of these single-use respirators [4,5]. Indeed, this practice is listed by the Centers for Disease Control and Prevention (CDC) as a crisis capacity strategy for when N95 supplies are low [3]. Such large-scale decontamination and reuse of N95 FFRs is unprecedented, and there is an urgent need for practical guidance on how to do so safely, effectively, and without compromising the performance N95 FFRs.

1.2 Rationale for the use of UV-C

The use of ultraviolet germicidal irradiation (UVGI) in healthcare settings has been well-documented in the literature and is used for room-level decontamination at many institutions. In these UVGI systems, UV-C irradiation is used to inactivate *Clostridium Difficile* (C. diff), *Methicillin Resistant Staph Aureus* (MRSA), and *Vancomycin Resistant Enterococci* (VRE) in hospital rooms [6]. This method works by generating dimers in DNA and RNA of exposed microorganisms, rendering them incapable of replication [7]. Within the context of this paper, "decontamination" will refer to, at minimum, a 3-log reduction of SARS-CoV-2 analogues (i.e., 99.9% inactivation), per FDA guidelines for N95 Tier 3 bioburden reduction [8]. Like most N95 decontamination procedures, this high-level disinfection method should be viewed as a risk mitigation strategy rather than complete sterilization.

The effectiveness of viral inactivation by UV-C depends on the delivered UV-C dose, which is a function of exposure time and irradiance, as well as the UV-C source wavelength, the ability of the microorganism to resist UV-C degradation, and the surface structure of the objects being decontaminated. In general, N95 respirators consist of several different layers of material with different optical properties. Filtration primarily takes place in two inner, electrostatically charged layers of spun polypropylene, which trap small aerosols by electrostatic attraction. Larger particles or droplets are filtered by mechanical blockage. The spun material is loosely packed in order to minimize the pressure drop across the material during user respiration. The filter layers are sandwiched between inner and outer layers which mechanically support the spun material and provide additional protection against larger droplets as well as fluid-resistance. The N95 designation implies that the FFR filters at least 95% of particles with a diameter of 300 nm. For SARS-CoV-2 contamination of N95 FFRs, a UV-C irradiation dose of 1.0-1.2 J/cm^2 or higher at both surfaces of the respirator is recommended to achieve decontamination [9]. N95 FFRs can be exposed to higher levels without apparent degradation, but damage is evident at levels exceeding 100 J/cm^2. These extremely high doses have been shown to cause a breakdown of the polypropylene fibers and a decline in respirator filtration and structural integrity and should be avoided [10]. At 1 J/cm^2 UV-C exposure dose, the number of re-use cycles is limited by mechanical wear and/or soiling of N95 FFRs, rather than cumulative UV-C exposure.

Some major advantages of UV-C over other decontamination methods include rapid throughput, ease-of-use, low electrical power requirements, absence of toxic or dangerous chemicals, and relatively simple overall device design and construction. UV-C methods are considered a decontamination process (3-log viral reduction) and not a sterilizing process (reaching at least 6-log viral inactivation and spore destruction). Therefore, it is strongly recommended that processed FFRs be indexed and returned to the initial user.

1.3 Scope of the paper

In this paper, we present evidence-based design principles for three different UV-C decontamination systems of N95 FFRs. The approaches were created with consideration for use in resource-constrained settings such as hospitals in low- and middle- income countries (LMICs) and rural healthcare facilities. The three designs provide easily constructed, cost-effective solutions, using generally widely available components, with sufficiently high throughput to meet the demands of hospitals, clinics, and first responders who face shortages of N95 FFRs.

An additional aim of the paper is to illustrate optical models and testing procedures which facilitate the design of instruments specifically for the application of N95 FFR decontamination. We want to stress that each manufacturers' N95 design should be considered unique with distinct optical and mechanical properties. The tests that we report here were primarily performed on the model #1860, manufactured by 3M, Inc. The biological and optical testing results provided in this paper establish practical solutions to decontamination problems, however the data we present here is specific to the 3M 1860. Sufficient design information is provided in this report and in the supplementary materials

(Supplement 1, sections 1-6) so that a reasonably skilled person with an optics background can modify, construct, validate, and operate the decontamination chambers using locally available resources (Supplement 1, sections 1-4).

We first present the general optical design methods for the decontamination chambers. We then describe in some detail the optical and mechanical properties specific to the 3M 1860 N95 FFR that are essential to consider for proper decontamination and to determine the suitability for reuse. These properties will likely differ depending on the FFR manufacturer and model. Finally, we describe the biological testing performed to demonstrate the level of decontamination achieved.

2. General design principles

UV-C photons, generally defined as having wavelengths in the range of 200-280 nm with germicidal activity peaking at around 265nm, have been shown to be particularly effective for decontamination of bacterial, viral, and fungal pathogens. N95 FFRs have an approximately hemispherical dome shape and an ideal decontamination chamber would illuminate the N95 FFR uniformly from all directions. Any chamber design needs to take into account the geometry of the most common UV-C sources: mercury UV-C lamps are cylindrical in shape and UV-C LEDs are essentially point sources. Disadvantages of UV-C LEDs include the need to produce diffuse and uniform exposure, much higher cost, and much lower efficiency than mercury discharge lamps. We have chosen to use UV-C lamps in our design since these sources are more widely available, can currently supply higher average powers, and are in general more cost effective than UV-C LEDs. A typical emission spectrum from a low-pressure mercury UV-C is shown in Fig. 1.

The lamps we use are specifically chosen to be non-ozone producing lamps with rapid start ballast power supplies, similar to those used in common fluorescent lamps (e.g. Philips model 30WT8). The appropriate choice of power supply ballast is particularly important to provide the longest possible lifetime for the UV-C lamp. The design objective can then be formulated as follows: given a desired throughput of N95 FFRs per day, design a containment chamber with sufficiently intense interior UV-C light sources such that the irradiance onto the N95 FFRs is uniform within 20%, a reasonable practical target, on the front, back and curved side surfaces of the N95 FFRs. This level of uniformity can be predicted using our ray trace models and verified by direct measurement using a properly designed irradiance meter (e.g. Thor Labs, Model PM100D console and S425C power sensor head). The UV-C units discussed here met this objective and provided a UV-C dose of at least 1 J/cm^2 to N95s in less than 5 minutes exposure time.

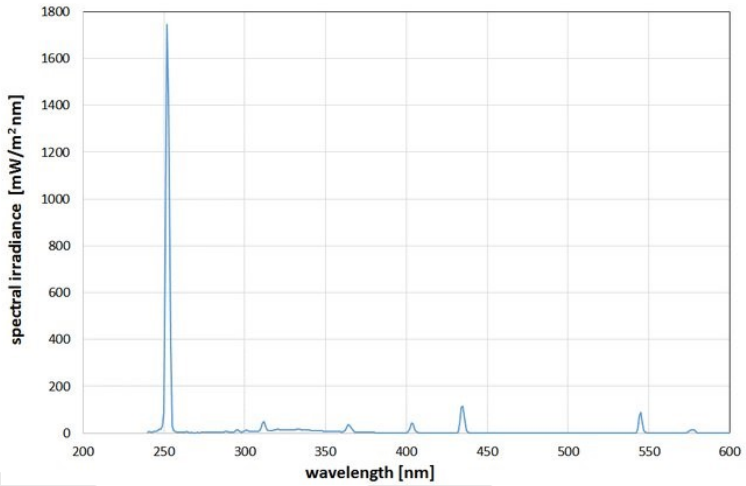

Fig. 1 Typical emission spectrum from a low-pressure mercury discharge germicidal lamp. The dominant emission is at 254 nm (~85%) with lower power emission (~15%) in the UV-B, UV-A and visible spectral regions. (©Schmid J, Hoenes K, Rath M, Vatter P, Hessling M. from "UV-C inactivation of Legionella rubrilucens," licensed under Creative Commons Attribution 4.0 License.)

After some preliminary studies and experiments we selected three configurations:

1. **The Horizontal Cabinet**: A rectangular cabinet in which N95 FFRs are illuminated from above and below (Fig. 2.)
2. **The Vertical Cabinet**: A rectangular cabinet with doors in which the N95 FFRs are placed in a vertical plane and illuminated from front and behind (Fig. 3.)
3. **The Cylindrical Design**: A cylindrical can in which the N95 FFRs are suspended from a frame located on the axis of the cylinder (Fig. 4.)

Fig. 2. Horizontal UV-C-decontamination chamber. The masks rest on a horizontal metal mesh support. A thin wire mesh (1-inch hexagon) was chosen as a tray to allow UV-C exposure on both sides while minimizing interference due to shadowing.

Fig. 3. Vertical cabinet with two front doors. The cabinet is a standard metal storage cabinet approximately 2 m high which was chosen to provide sufficient height to accommodate an upper and lower bank of UV-C lamps. The upper and lower banks are offset to fit into the cabinet and have a small region of overlap which does not appear to materially impact the vertical intensity profile in the cabinet. The CAD model illustrates a supporting frame containing 28 masks in 7 rows of 4. We estimate up to 40 masks could be loaded per UV-C exposure procedure in this design.

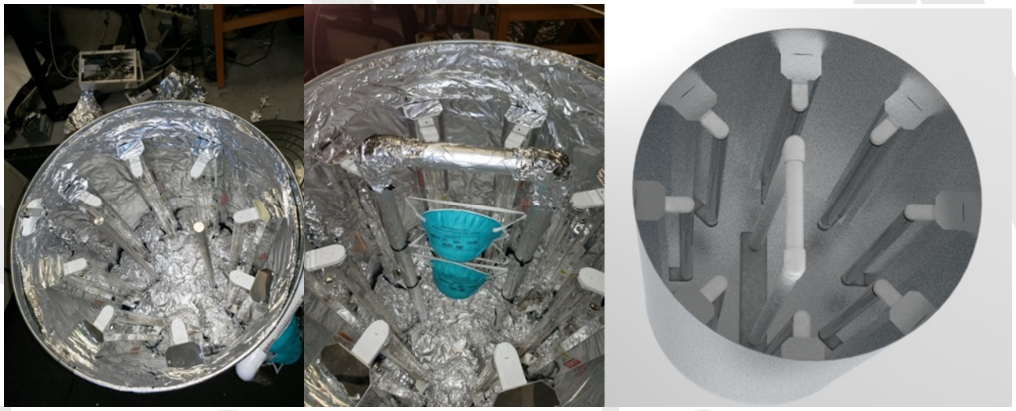

Fig. 4. Cylindrical design chamber. The chamber can hold up to 4 masks in the central support frame.

Table 1. Decontamination chambers investigated in this research.

Design	Shape	Size	Throughput/day	US Cost
The horizontal cabinet	Rectangular horizontal tray	H 18" x W 24" x D 36"	4300	~$1500
The vertical cabinet	Rectangular vertical cabinet	H 72" x W 36" x D 24"	5000	~$1500
The Cylindrical design	Cylindrical container	D 20" x H 27"	1500	~$750

Tradeoffs needed to be made regarding chamber size, N95 FFR throughput, cost, availability of local materials, safety, ozone levels, reliability, fluence levels, and isotropy of illumination. The cylindrical geometry of the UV-C lights dictates mounting them on a flat or

cylindrical surface, with coatings that reflect and diffuse emitted light to create an isotropic irradiance in the exposure area. Aluminum foil is a low cost and widely available material that can be draped over or bonded to the interior chamber walls, providing higher uniformity and irradiance due to an approximately 73% reflectivity at 254 nm UV-C wavelengths [11]. The N95 FFRs themselves diffusively reflect, scatter, and transmit UV-C illumination and careful consideration must be given to account for the effect of the N95 FFRs on the overall irradiance level inside the cabinets or container, in particular to avoid shadowing of adjacent N95s. As this information is not readily publicly available, we carried out an investigation to obtain these data for OpticStudio by Zemax (www.Zemax.com) modeling by measuring N95 optical parameters directly. The N95 FFRs should be geometrically arranged to avoid any obvious obstruction of light by adjacent masks, straps, or suspension systems.

3. Optical Models of the Designs

OpticStudio modeling is a well-established optical design tool and widely available in high-income countries, but less so in LMICs. We therefore decided to apply a first order estimate of the design using a simplified analytical approach, without resort to OpticStudio modeling [12]. These first-order calculations are a reasonably close approximation to using OpticStudio tools, but do not include the effects of reflective walls in the enclosure. This approach would allow someone with an optics background to quickly estimate the performance of alternative lamp placements in a variety of chamber geometries and arrive at a useful estimate of the illumination levels necessary for decontamination of N95 FFRs.

3.1 Geometrical Optical Models for UV-C Linear Sources

Most common UV-C sources are cylindrical lamps with a length 20 to 50 times their diameter emitting approximately 90% UV-C at 254 nm and about 10% in the UV-A, UV-B and visible portion of the spectrum. These sources are best modeled as cylindrical, linear light diffuse-emitting light sources. Of the available linear models, the view factor model seems to be the most accurate at estimating irradiance for a given point of interest. The view factor model assumes that the UV-C source is a homogeneous cylinder. Fig. 5 provides a visual aid for the formulas corresponding to the view factor model shown below. Once the irradiance is computed, exposure time is deduced by requiring that the total irradiance flux equals 1J/cm^2. Total irradiance at any point inside the decontamination chamber is computed by superposition of irradiance from all incident sources, projected onto the measurement surface. The following equation only apply to a point of interest located at the end points of the lamps and do not factor in the effects of reflectivity of various surfaces inside the chamber. To compute the view factor for a point located at any position along the lamp (i.e. not coplanar with an end of the lamp), it must be divided into two segments with the power split proportionally amongst those segments.

The full view factor equation is described fully and is summarized in the supplementary materials (Supplement 1, section 6) [12]. The equation can be simplified significantly with a few assumptions, providing a simple estimate of the direct irradiance from an array of UV-C lamps at a specified distance directly across from the array. In the limits where the cylinder length is much greater than the distance to the illumination point and the diameter of the lamps, the view factor model effectively reduces to the emission expected from an infinitely long cylindrical source. The irradiance can be estimated from the Keitz equation [12]. Let P be the tubular lamp UV power (W), L is the tube length (cm), D is the distance to the N95 mask (cm), and R is the tube radius (cm). When L/R>20 and D/R <15 the irradiance is approximately

$$E = \frac{P}{4\pi LD}\ \frac{W}{cm^2} \qquad (1)$$

The irradiation time is t = dose/E where dose is the required J/cm^2 to inactivate the virus (typically 1 J/cm^2). In other words, for all instances where L/R>20 and D/R<15, the full view factor equation as shown in the supplementary materials (Supplement 1, section 6) can be simplified down to eq(1) to within 5% accuracy. The contributions of multiple lamps can be accounted for by simply adding the levels predicted by eq. (1) for each lamp location.

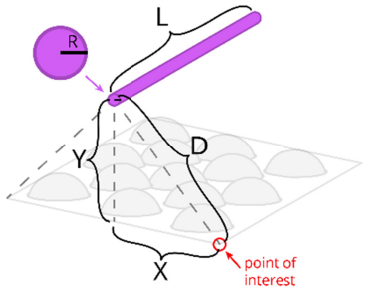

Fig. 5. Example illumination geometry for rectangular chambers

Equation 1 provides a simple first-order estimate of the irradiance from an array of cylindrical UV-C sources without including the effects of reflections in the chamber. In practice, reflections from walls and other surfaces need to be taken into account, as well as detailed considerations of geometry to account for a proper calculation of irradiance. In particular, proper modeling of irradiance incident on the mask needs to take into consideration the shape of the mask and its optical properties such as absorption, reflection and transmission coefficients. We include these effects in the OpticStudio modeling results and compare our models against experiments for the three cabinet designs described above.

3.2 Ray Trace Simulation Models

The formula in eq. (1) can be used to reasonably estimate direct irradiance from a UVGI lamp array, but we recommend that design models use computational optical ray tracing to achieve the most accurate results [12]. The software used by the authors for the models in this paper is OpticStudio and the simulations were run in purely non-sequential mode. Details of the optical model are discussed in [13]. The following assumptions were used for the OpticStudio modeling, based on experimental data:

Aluminum foil: 73% reflectivity: 30% specular, 70% diffuse

Paint on walls: 7% reflectivity: 30% specular, 70% diffuse

Bare walls: 7% for non-foil (30% specular, 70% Lambertian for both instances)

Lamp fixture reflectivity: 80% (100% specular).

N95 FFR mask: CAD model that is approximately hemispherical shape with 1% transmission through all layers, 94% absorbance, and 5% reflectivity: 0% specular, 100% diffuse

3.2.1 Characterizing N95 FFR Optical Properties

N95 FFRs trap viral particles within a polypropylene filter layer, not at the N95 surface where UV-C is incident. We examined whether sufficient UV-C penetrates N95s to inactivate virus trapped within the filter. To the best of our knowledge the detailed optical properties of an N95 mask have not been measured previously. For optical modeling purposes and to assess the potential for decontamination below the surface of N95s, we need to know the optical transmission, reflection, and absorption coefficients for the N95 FFR. Therefore, we set out

to investigate the optical properties of N95 FFRs and developed OpticStudio models to design close to isotropic fluence levels incident on batches of N95 FFRs. Using an integrating-sphere spectrophotometer we measured diffuse transmission spectra of the layers and assumed about the reflectivity of the layers, which compared well with experiments, using the parameters noted in section 3.2. It is important to note that the optical properties of the N95 FFRs listed in Fig. 6 are specific to these versions and other types of N95 FFR masks will likely have different optical characteristics.

As mentioned, the geometric shape of an N95 FFR is roughly hemispherical and thus its internal and external surfaces are oriented at a variety of angles making it a unique problem for optical modeling. To better characterize the behavior of an N95 FFR in the presence of UV-C light, all four layers of a single N95 FFR (3M 1860S) were carefully dissected and the diffuse UV transmission through each layer was measured Fig. 6. The results of this study showed that the transmission of UV-C light through all layers of the N95 FFR was 1-2%. With illumination from both sides, the front three layers combined transmit 6.2% the UV-C light and the back most layer transmits 15.3% of the light. This effectively means that the core of the respirator receives 21.5% of the UV-C dose delivered at the surface and that all layers receive at least this level of exposure, *provided the respirators are illuminated from both sides*. Another N95 FFR was tested (Gerson 1730) and the UV transmittance measured within its layers was similar at 18.8%. We developed an optical model of the N95 FFR based on a 3D CAD reconstruction and included the geometrical and optical properties of the N95 FFR in our ray trace simulations.

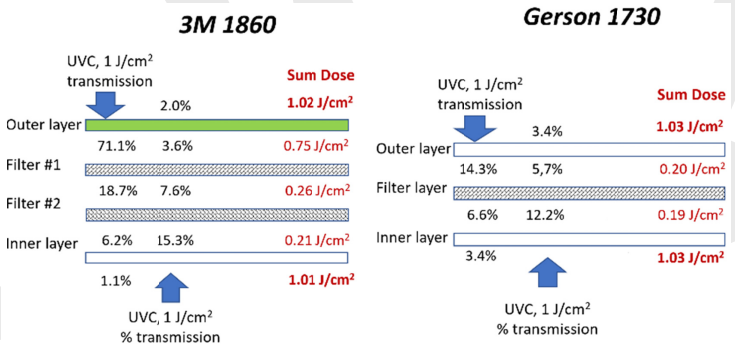

Figure 6: Dissecting and measuring the transmission through each layer of two N95 FFRs, the 3M 1860S and the Gerson 1730. This shows the importance of illuminating the respirators from both sides.

3.2.2 Ray Trace Model Results

Ray tracing results using the design parameters noted above were compared against calculations and direct measurements for all three decontamination chambers. The results are shown in Fig. 7-9. Details of these designs and the measurement procedures used to characterize their performance are contained in supplementary materials (Supplement 1, sections 1-3).

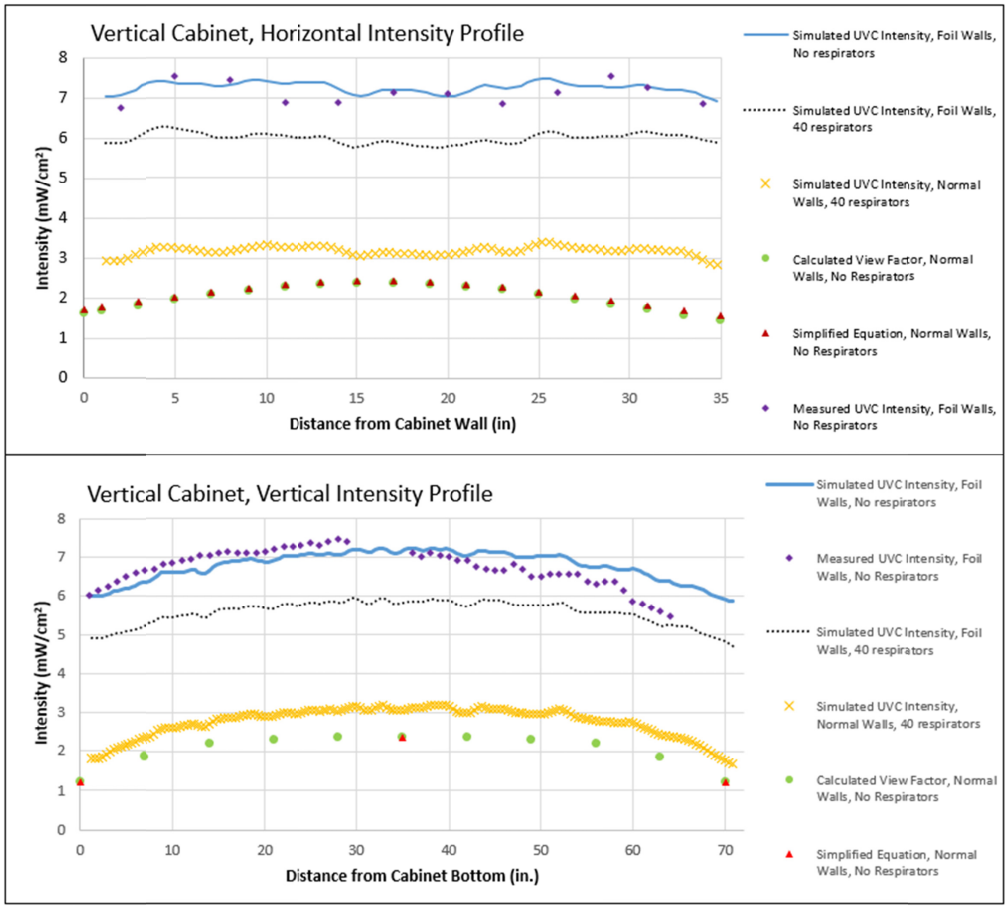

Fig. 7. Measured and simulated intensity profiles within the Vertical Cabinet. The measurements were made with the doors closed and no masks in the chamber. (Supplement 1, section 2) The optical model was run with both and empty and fully loaded chamber (40 FFRs) to illustrate the impact of the additional absorption due to the presence of the FFRs in the chamber.

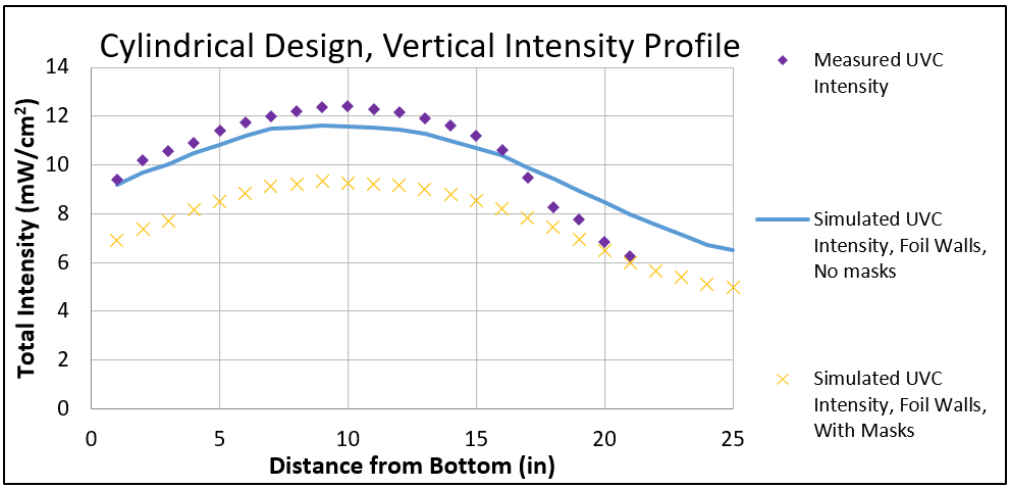

Fig. 8. Measured and simulated intensity profiles within the Cylindrical Design. There is approximately a two-fold change in the intensity profile. The decontamination exposure time should be determined by the minimum level of intensity exposure. (Supplement 1, section 3.)

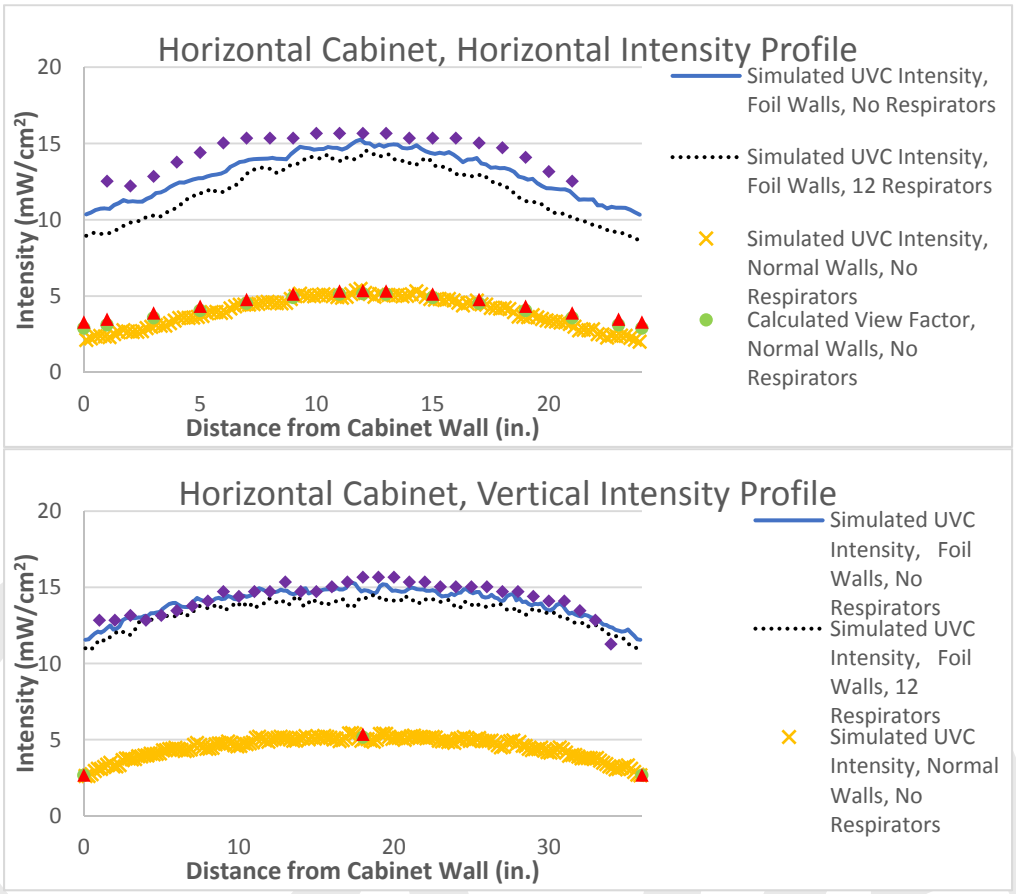

Fig. 9. OpticStudio ray trace model and measured intensity profiles of the Horizontal Cabinet. (Described further in Supplement 1, section 1.)

The data were found to be in good agreement with the ray trace models, and variations between the model and measurements can likely be attributed to imperfections in the non-smooth, foil-lined walls, and the reproducibility of the placement of the power meter inside the closed cabinet during the measurements. We note that our models indicate that the addition of masks reduces the intensity by about 15% compared to empty containers. Furthermore, the simulation with the aluminum foil lined walls saw a two-fold or greater increase in irradiance over the model simulating simple paint, consistent with our measurements, further emphasizing the utility of using aluminum foil as a simple means to increase radiant intensity on the masks.

4. Operational System Performance

4.1 Bacillus pumilus Spore Testing

The UV-C sensitivity of various microorganisms including bacteria, bacterial spores, mold spores, and viruses is well studied in the literature [12]. The following biological inactivation study uses a highly UV-C resistant bacterial spore, *Bacillus pumilus* (PM-106, Crosstex), as a surrogate for SARS-CoV2. These spores are generally used for radiation sterilization processes and are notoriously resistant to ultraviolet light [14]. In one study, a certain strain of *Bacillus pumilus* required a dose of nearly 0.350 J/cm^2 to achieve 4 log inactivation [15]. In the biological tests used in this paper, the bacteria spore strips are loaded with 2.8x10^6 C.F.U.

by the manufacturer, which results in a more than 6 log inactivation measurable with this assay. The spore strips were exposed to UV-C radiation, up to 1 J/cm^2, flat or perpendicular to the UV-C light source to mimic the different surface contours of the mask. The strips are placed in growth media containing a pH indicator dye and incubated for 2 to 7 days. Any residual viable bacteria will grow in the media resulting in a change in the media pH which causes a concomitant change in color of the pH indicator from purple to yellow. The positive control (no UV-C radiation) displayed a color change to yellow while spores treated with UV-C doses as low as 200 mJ/cm^2 up to 1 J/cm^2 did not show a color change, implying a 6-log bacteria spore inactivation at those doses. The test was repeated under the same conditions with the bacteria spore strips "sandwiched" between the layers of two N95 FFRs, effectively simulating an entire respirator on each side of the strips. After a single UV-C surface dose of 1 J/cm^2, all locations showed a 6-log inactivation of the bacteria spores. Both experiments were repeated three times with identical findings Fig. 10.

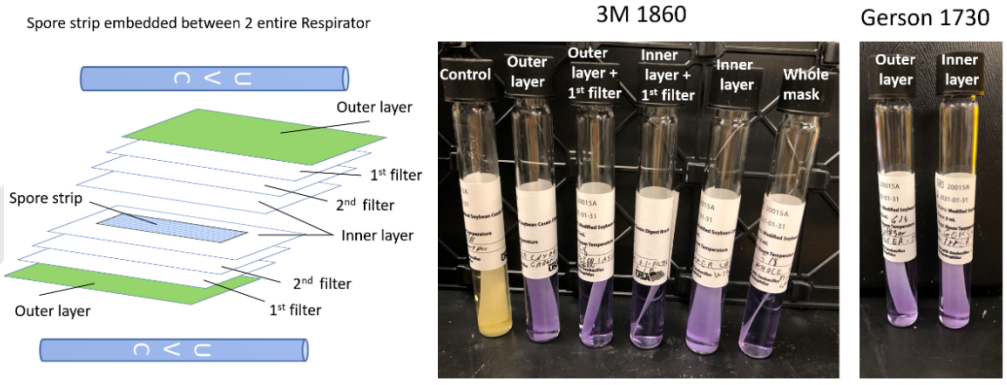

Figure 10: Biological inactivation of *Bacillus Pumilus* spores. A 6-log reduction is shown after 7 days of incubation. The change in color from purple to yellow is due to a chemical indicator which detects a change in the pH of the growth media, which occurs due to any bacterial growth during the 7-day incubation period.

4.2 Mechanical N95 FFR Testing

N95 FFRs use a non-woven layer of electrostatically charged melt blown polypropylene-based filters to capture airborne particles [16]. The N95 classification refers to the masks' ability to filter ≥95% of non-oil-based particles of any size greater than 0.300 microns in size, while also being able to filter out smaller particles as well via the electrostatic charge on the polypropylene fibers. Filtration of larger particles (diameters of several microns and higher) occurs through trapping or mechanical blockage of the particles within the melt-blown filter layers. For reference, the diameter of a coronavirus is approximately 0.12 microns, the size of a typical bacterium is a cylinder roughly 1 micron in diameter and several microns long. Typical droplet sizes range from 10 microns to a millimeter and aerosols are generally considered to range from several hundred nanometers to 10 microns. The N95 FFR contours to the human face, sealing as tightly as possible around the nose and mouth and necessitating all inhaled air to flow through, rather than around, the respirator. The mask is held in place by two elastic bands placed around the top of the head and neck which supply the pressure required to seal the mask to the face of the wearer.

The balance between achieving suitable N95 FFR decontamination without compromising intrinsic fit and filtration properties is a very delicate one. Many different approaches already exist for general purpose biological decontamination in healthcare settings, but virtually all of them compromise respirator integrity. Therefore, it is important that any new approach for N95 FFR decontamination include a proper assessment of intrinsic mask properties to make sure that they have not been compromised. The approaches outlined in this paper have proven

to have no significant deviation for fit, filtration, and strap elasticity through five cycles of decontamination for a common N95 FFR model (3M 1860S) that was tested, as shown in Table 2.

Table 2: The results of the filtration test of an N95 FFR (3M 1860S) shows no significant mask deterioration for up to 5 cycles of 1 J/cm^2. Results are shown for 5, 2 and 1 decontamination cycles. The exposures were performed in the horizontal cabinet pictured described above.

Treatment	Airflow (LPM)	Resistance (mmH_2O)	Penetration (%)
Control	85.0	11.7 ± 0.7	0.8 ± 0.2
5 x 1 J/cm^2 UV-C	85.0	10.1	0.19
5 x 1 J/cm^2 UV-C	85.0	10.7	1.23
5 x 1 J/cm^2 UV-C	85.1	9.6	0.79
2 x 1 J/cm^2 UV-C	85.0	9.5	1.36
2 x 1 J/cm^2 UV-C	85.1	9.1	0.80
2 x 1 J/cm^2 UV-C	85.1	11.0	0.79
1 x 1 J/cm^2 UV-C	85.3	10.1	1.01
1 x 1 J/cm^2 UV-C	85.3	11.1	1.09
1 x 1 J/cm^2 UV-C	85.5	11.3	1.17

5. Operational Cautions

5.1 UV Exposure Warning

Exposure to UV-C irradiation carries human health risks, particularly to the skin and eyes. Painful acute conjunctivitis can result from doses >5 mJ/cm^2, which is less than 1% of the target dose for mask decontamination of 1 J/cm^2. Proper device design and operator precautions are therefore required to avoid UV-C exposure to the eyes. Skin exposure of >10 mJ/cm^2 results in mild redness, desquamation, and pigmentation. There is no evidence in humans of UV-C-induced skin cancer, but this is a possible long-term hazard [17].

5.2 Ozone

A common concern surrounding the use of UV-C is the production of ozone. Ozone can be generated by UV photons in the range of 180-220 nm. Some versions of low-pressure mercury lamps are specifically designed using quartz materials that also transmit vacuum ultraviolet light at 185 nm which can generate significant amounts of ozone. Ozone can pose an additional health hazard to the operator, particularly when generated and accumulated in closed cabinet designs where ozone can be trapped during the decontamination procedure. Therefore, the low-pressure mercury lamps used for decontamination should be non-ozone producing.

To confirm the absence of ozone exposure to the end user for standard germicidal lamps used in most UV-C decontamination devices, an ozone detector (Aeroqual model 300 with 0.5 ppm detector) was placed inside the Vertical Cabinet and measurements were taken during a typical decontamination procedure lasting 10 minutes. During this operation no ozone was detected within the Vertical Cabinet. The Horizontal cabinet achieved similar results. In both designs, under normal use, the ozone levels were below the limit of detection of the sensor, (0.001ppm) and well below the minimum acceptable exposure levels over an 8-hour period (0.070ppm) as defined by the EPA [18]. We additionally measured ozone levels outside the cabinet and inside the Horizontal Cabinet before the unit was switched on as well as inside during the UV-C cycle and right afterwards. There was significant reduction in ambient

ozone levels after the experiment. The baseline ozone level was about 0.007 ppm prior and 0.000 during and after cycle, Fig. 11.

Ozone absorbs 254 nm UV-C, undergoes photochemical decomposition and recombination to yield molecular oxygen, which explains our measurements. To further confirm this explanation and the absence of ozone exposure to the end user for standard germicidal lamps used in most UV-C decontamination devices, the ozone detector and an ozone generating lamp (OZN-1. R & M Supply, Inc. Perris, CA) were placed inside the Vertical Cabinet and the ozone generator allowed to run for about 30 seconds. The ozone generating lamp was then turned off and the decay over time was measured and graphed, Fig. 12. The time constant was found to be 2500 seconds with all 16 UVGI lamps turned off but only 33 seconds with the UVGI lamps turned on. This confirms that the UVGI lamps used are effective at photodissociation of the ozone. Therefore, it appears that a closed cabinet design is likely superior to flowing air through the chamber or having an open design where the ozone can diffuse out of the irradiation area.

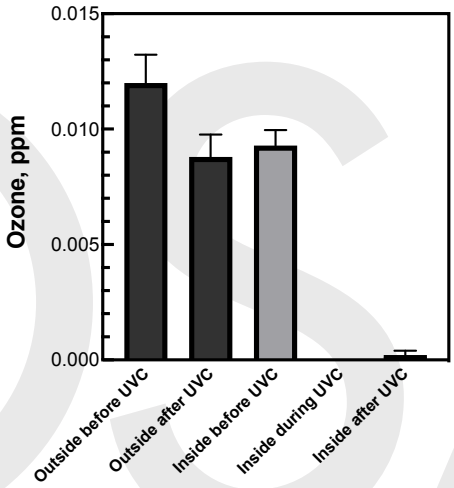

Fig. 11. Graph showing that during decontamination cycles, the ozone levels are below the limit of detection of the sensor in the horizontal cabinet.

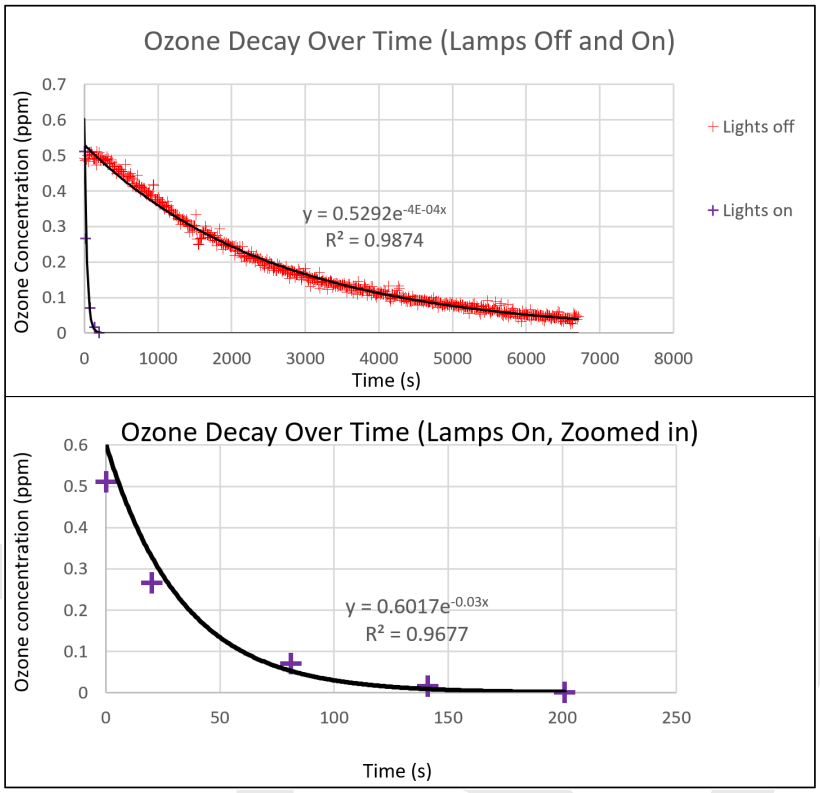

Fig. 12. Graphs showing that the UV-C lamps quickly eliminate any ozone in the cabinet that might be generated during the decontamination process.

5.3 Strap Decontamination

Reports have demonstrated that under certain conditions, there may be residual virus on N95 FFR straps post UV-C exposure, likely due to portions of the N95 FFR straps being shielded from the UV-C light. This suggests the need for supplementary decontamination of the straps (9). Therefore, it is recommended to wipe down N95 FFR straps with a compatible disinfectant after completing a UVGI exposure cycle [19]. Examples of common compatible disinfectants include hydrogen peroxide, 70% isopropyl alcohol, or ethanol [20]. If this additional step is employed, extra caution should be used to avoid touching the N95 FFR facepiece as common disinfectant chemicals can degrade N95 FFR function [21].

5.4 Soiling

Soiling has been found to reduce UV-C inactivation efficacy of both MS2 bacteriophage from N95 FFRs [22] and *C. difficile* spores from glass and plastic surfaces [23]. Materials deposited on the respirator surface such as sebum, cosmetics, blood, and sunscreen may block UVGI light, hindering decontamination. As a general note, cosmetics, skin creams, or other barriers should not be worn during respirator use. Any N95 FFR found to be soiled with such products, or externally contaminated with visible blood or body fluids, should be discarded, and not undergo decontamination.

5.5 Temperature and humidity

High humidity can decrease UV-C efficacy on generic surfaces [24] and on the surfaces of N95 FFRs [22]. Considering that N95 FFRs are being worn for lengthy periods of time to extend their use, it is not unreasonable to assume that the constant breathing and sweat they are exposed to throughout the day will moisten them. However, while the effect of humidity on microorganism survival is significant for bacterial species, it is practically negligible for viruses [12]. Furthermore, the humidity over time was measured within the vertical cabinet and was found to be low, presumably due to the higher internal temperature of the cabinet Fig. 13. The mild heat produced by the UV-C fixtures was enough to functionally act as a drying step for the N95 FFRs, but not too much as to cause damage to the respirators. However, further investigation on this matter is warranted to assess the viability of microorganisms on the surface of N95 FFRs exposed to UV-C in humid conditions.

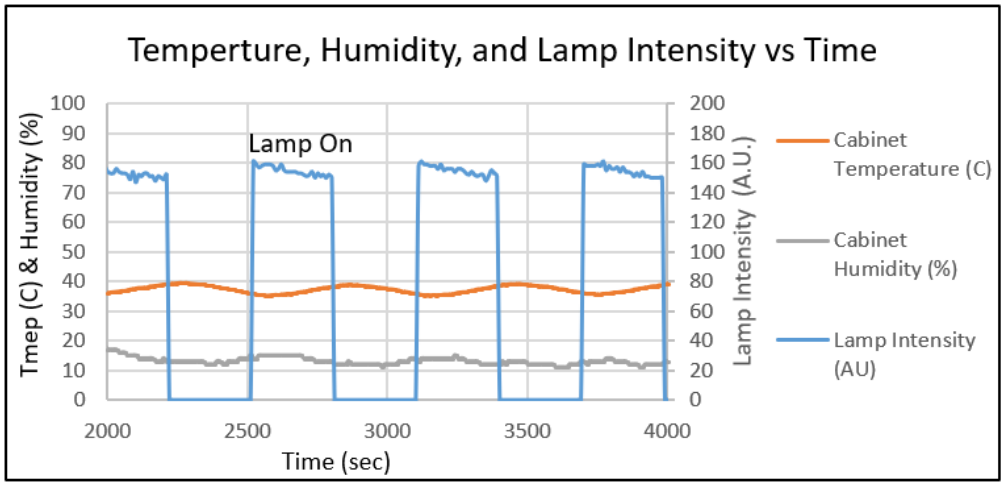

Figure 13: Temperature and humidity data over several cycles of the Vertical Cabinet. Neither the temperature nor the humidity approaches the thresholds that have been documented to damage N95 FFRs. The chamber was cycled 150 times, with the lamps on for 320 s and then off for 320 s, with no observable change in the lamp peak intensity. The data shown was taken after approximately 5 cycles. For the Horizontal Cabinet the temperature rise with sustained operation at 50% duty cycle was similar, less than 5 C. The graphs indicate less than 10% change in the lamp intensity during a typical decontamination cycle, primarily due to the increase in temperature inside the chamber.

6. Conclusions and Future Work

We present in this report evidence on the efficacy of properly designed UV-C instruments for decontamination of N95 FFRs. However, there is still a need for further research regarding the inactivation specifically of SARS-CoV2 droplets deposited on respirator surfaces. We are currently conducting studies to measure direct viral and spore inactivation with microorganisms directly inoculated on the surface and within the layers of an N95 FFR. It should be noted that ultraviolet germicidal activity hinges directly on the medium that the microorganism resides on. Given the global shortage of N95 FFRs and equivalents, the ability to run a large-scale study with a statistically significant number of samples would be difficult to conduct at this time.

Finally, it is critical to understand that any decontamination procedure is a risk mitigation strategy, currently warranted in critical FFR shortage situations, not a long-term solution to shortage of PPE. Anyone interested in duplicating the devices described in this manuscript should follow certification guidelines recommended by the relevant regional regulatory authorities.

Acknowledgements

We thank our fellow members of the N95DECON.org collaboration who have provided very useful reviews of the current literature on decontamination procedures. We would like to thank Manu Prakash for his leadership in organizing the N95DECON collaboration and for his enthusiastic support and encouragement of this research.

Funding

N.S. is supported by National Institutes of Health (NIH) grant T32 DK7573-29

Disclosures

ME has ownership in a small amount (10 shares) of 3M stock.

References

1. Megan L. Ranney, Valerie Griffeth, and Ashish K. Jha. Critical Supply Shortages — The Need for Ventilators and Personal Protective Equipment during the Covid-19 Pandemic. The New England Journal of Medicine. March 25, 2020.
2. Recommended Guidance for Extended Use and Limited Reuse of N95 Filtering Facepiece Respirators in Healthcare Settings. [Online], Center for Disease Control and Prevention, https://www.cdc.gov/niosh/topics/hcwcontrols/recommendedguidanceextuse.html [Cited: July 8, 2020.]
3. CDC. Strategies for Optimizing the Supply of N95 Respirators. [Online] Centers for Disease Control and Prevention, April 2, 2020. [Cited: June 24, 2020.] https://www.cdc.gov/coronavirus/2019-ncov/hcp/respirators-strategy/index.html.
4. B. Kaiser and T. Hsu. Where Thousands of Masks a Day Are Decontaminated to Battle the Virus. The New York Times. April 11, 2020.
5. G. Kolata. As Coronavirus Looms, Mask Shortage Gives Rise to Promising Approach. The New York Times. March 20, 2020.
6. Katelyn C. Jelden, Shawn G. Gibbs, Philip W. Smith, Angela L. Hewlett, Peter C. Iwen, Kendra K. Schmid and John J. Lowe, "Comparison of hospital room surface disinfection using a novel ultraviolet germicidal irradiation (UVGI) generator, Journal of Occupational and Environmental Hygiene, 13:9, 690-698. July 15, 2016.
7. Nicholas G. Reed, "The History of Ultraviolet Germicidal Irradiation for Air Disinfection," Public Health Reports, Vol. 125, pp. 15-27. January 1, 2010.
8. U.S. Department of Health and Human Services. Recommendations for Sponsors Requesting EUAs for Decontamination and Bioburden Reduction Systems for Surgical Masks and Respirators during the Coronavirus Disease 2019 (COVID19) Public Health Emergency. [Online] May 2020. [Cited: June 18, 2020.] https://www.fda.gov/media/138362/download.
9. Brian Heimbuch and Del Harnish, Research to Mitigate a Shortage of Respiratory Protection Devices During Public Health Emergencies. [Online] September 30, 2020. [Cited: June 24, 2020.] https://www.ara.com/sites/default/files/MitigateShortageofRespiratoryProtectionDevices_3.pdf.
10. William G. Lindsley, Stephen B. Martin Jr., Robert E. Thewlis, Khachatur Sarkisian, Julian O. Nwoko, Kenneth R. Mead, and John D. Noti, "Effects of Ultraviolet Germicidal Irradiation (UVGI) on N95 Respirator Filtration Performance and Structural Integrity," Journal of Occupational and Environmental Hygiene, 12:8, 509-517. July 1, 2015.
11. Rajul Randive. Using UV Reflective Materials to Maximize Disinfection. [Online] June 16, 2020. [Cited: June 24, 2020.] https://www.klaran.com/images/kb/application-notes/Using-UV-Reflective-Materials-to-Maximize-Disinfection---Application-Note---AN011.pdf.
12. Wladyslaw Kowalski. Ultraviolet Germicidal Irradiation Handbook: UVGI for Air and Surface Disinfection. New York: Springer, 2009.

13. Jeffrey P. Wilde, Thomas M. Baer, and Lambertus Hesselink, Modeling UV-C Irradiation Chambers for Mask Decontamination using Zemax OpticStudio (Submitted for publication)
14. David A. Newcombe, Andrew C. Schuerger, James N. Benardini, Danielle Dickinson, Roger Tanner, and Kasthuri Venkateswaran, "Survival of Spacecraft-Associated Microorganisms under Simulated Martian UV Irradiation," Applied Environmental Microbiology, Dec 2005, 71 (12) 8147-8156.
15. L. Link, J. Sawyer, K. Venkateswaran and W. Nicholson, "Extreme Spore UV Resistance of Bacillus pumilus Isolates Obtained from an Ultraclean Spacecraft Assembly Facility," Microbial Ecology, 47 (2), 159-163.
16. Lei Liao, Wang Xiao, Mervin Zhao, Xuanze Yu, Haotian Wang, Qiqi Wang, Steven Chu, and Yi Cui, "Can N95 Respirators Be Reused after Disinfection? How Many Times?" ACS Nano 2020, 14 (5), 6348-6356.
17. Joseph Cavallo and Vincent A DeLeo, "Sunburn," April 1986, Dermatologic Clinics, 4 (2), 181-187.
18. EPA. Eight-Hour Average Ozone Concentrations. [Online] United States Environmental Protection Agency. [Cited: June 24, 2020.] https://www3.epa.gov/region1/airquality/avg8hr.html#:~:text=Based%20on%20extensive%20scientific%20evidence,over%20an%208%2Dhour%20period.
19. Devin Mills, Delbert A. Harnish, Caryn Lawrence, Megan Sandoval-Powers, and Brian K. Heimbuch, "Ultraviolet germicidal irradiation of influenza contaminated N95 filtering facepiece respirators," American Journal of Infection Control, 46 (7), e49-e55.
20. EPA. List N: Disinfectants for Use against SARS-CoV-2 (COVID-19). [Online] United States Environment Protection Agency, June 24, 2020. [Cited: June 24, 2020.] https://www.epa.gov/pesticide-registration/list-n-disinfectants-use-against-sars-cov-2-covid-19.
21. Larry Chu and Ami Price, Addressing COVID-19 Face Mask Shortages. [Online] March 25, 2020. [Cited: 24 2020, June.] https://stanfordmedicine.app.box.com/v/covid19-PPE-1-2.
22. Myung-Heui Woo, Adam Grippin, Diandra Anwar, Tamara Smith, Chang-Yu Wu, Joseph D. Wander, "Effects of Relative Humidity and Spraying Medium on UV Decontamination of Filters Loaded with Viral Aerosols," Applied and Environmental Microbiology, 78 (16), pp. 5781-5787.
23. Rhiannon Wallace, Marc Ouellette, and Julie Jean, "Effect of UV □C light or hydrogen peroxide wipes on the inactivation of methicillin□resistant Staphylococcus aureus, Clostridium difficile spores, and norovirus surrogate," Journal of Applied Microbiology, 127 (2), 586-597.
24. Chun-Chieh Tseng and Chih-Shan Li, "Inactivation of Viruses on Surfaces by Ultraviolet Germicidal Irradiation," Journal of Occupational and Environmental Hygiene, 4 (6), 400-405. November 7, 2007.